Stem Cell Reports
Article

ISSCR

OPEN ACCESS

Deriving Dorsal Spinal Sensory Interneurons from Human Pluripotent Stem Cells

Sandeep Gupta,[1,2,5] Daniel Sivalingam,[1,2,5] Samantha Hain,[1,2,4] Christian Makkar,[1,2,4] Enrique Sosa,[2,3] Amander Clark,[2,3] and Samantha J. Butler[1,2,*]

[1]Department of Neurobiology
[2]Eli and Edythe Broad Center of Regenerative Medicine and Stem Cell Research
[3]Department of Molecular, Cell and Developmental Biology
University of California, Los Angeles, Los Angeles, CA 90095, USA
[4]CIRM Bridges to Research Program, California State University, Northridge, CA, USA
[5]Co-first author
*Correspondence: butlersj@ucla.edu
https://doi.org/10.1016/j.stemcr.2017.12.012

SUMMARY

Cellular replacement therapies for neurological conditions use human embryonic stem cell (hESC)- or induced pluripotent stem cell (hiPSC)-derived neurons to replace damaged or diseased populations of neurons. For the spinal cord, significant progress has been made generating the *in-vitro*-derived motor neurons required to restore coordinated movement. However, there is as yet no protocol to generate *in-vitro*-derived sensory interneurons (INs), which permit perception of the environment. Here, we report on the development of a directed differentiation protocol to derive sensory INs for both hESCs and hiPSCs. Two developmentally relevant factors, retinoic acid in combination with bone morphogenetic protein 4, can be used to generate three classes of sensory INs: the proprioceptive dI1s, the dI2s, and mechanosensory dI3s. Critical to this protocol is the competence state of the neural progenitors, which changes over time. This protocol will facilitate developing cellular replacement therapies to reestablish sensory connections in injured patients.

INTRODUCTION

The somatosensory system mediates the perception of touch (mechanosensation), pain (nociception), heat (thermosensation), and the position of the body in space (proprioception). These modalities enable us to perceive and react to the environment; they are thus essential for both well-being and survival. Somatosensory information is received peripherally, and then decoded centrally by interneurons (INs) in the dorsal spinal cord (Butler and Bronner, 2015), which relay sensory information to higher-order centers in the brain, including motor systems in the brainstem and cerebellum (Bermingham et al., 2001), as well as to motor output from the spinal cord. Distinct classes of sensory INs arise during embryonic development: they are classified as dorsal interneuron (dI)1 to dI6s. These neurons have different functional modalities, and arise via distinct developmental programs in different positions in the spinal cord (Lai et al., 2016). For example, the dI1s mediate proprioception (Yuengert et al., 2015). They are born from the dorsally located ATOH1$^+$ (Math1) neural progenitors (Helms and Johnson, 1998), and migrate to deeper position in laminae V-VII of the adult spinal cord upon maturation (Lai et al., 2016). Similarly, the dI2s and dI3s are derived from the NGN1$^+$ and ASC1$^+$ (Mash1) progenitors, respectively (Helms et al., 2005), and settle in distinct layers of the mature spinal cord. The dI3s mediate touch-activated motor behaviors (Bui et al., 2013), while the functions of the dI2s are currently unknown.

Spinal cord injuries (SCIs) can affect both sensory and motor systems and are debilitating emotionally and physically. SCIs are estimated to affect over 1 million people in the US, reducing their quality of life and costing ~$40 billion annually in health care (Armour et al., 2016). SCIs were considered intractable until pluripotent stem cells emerged as a remarkable reagent for understanding disease mechanisms, serving as a platform for drug screening, and providing a source of tissue for cellular replacement therapies. Important milestones toward treating SCIs have been the establishment of protocols to derive spinal motor neurons (MNs) from mouse (m) and human (h) embryonic stem cells (ESCs) (Li et al., 2005; Wichterle et al., 2002) and induced pluripotent stem cells (iPSCs) (Dimos et al., 2008; Karumbayaram et al., 2009). Stem cell-derived MNs have provided an important window into understanding of the pathology of motor diseases, such as amyotrophic lateral sclerosis (Sances et al., 2016) and spinal muscular atrophy (Ebert et al., 2009), as well permitting cellular replacement in injury models (Harper et al., 2004; Thomsen et al., 2014). While these advances raise the possibility of repairing motor functions in SCI patients, relatively little attention has been given to the recovery of sensory circuits that enable the patient to interpret their sensory environment and modulate motor output. In particular, no directed differentiation protocol

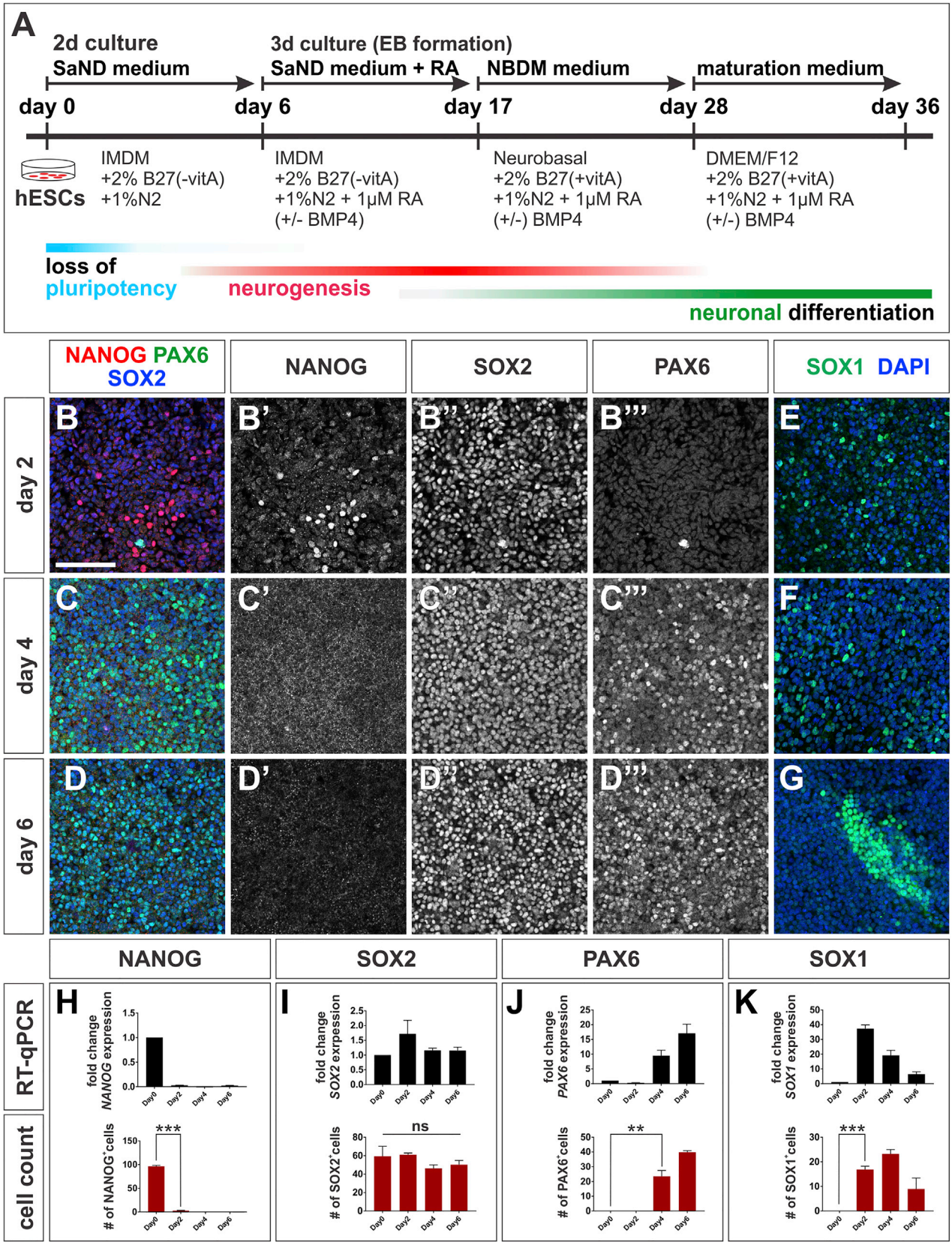

(legend on next page)

currently exists to generate sensory spinal INs from human pluripotent stem cells, the critical first step toward recovering somatosensation in SCI patients.

Toward this goal, we have developed a directed differentiation protocol that generates three key populations of dorsal sensory INs: the dI1s, dI2s, and dI3s. This protocol co-opts the developmental mechanisms that first establish these neurons in the embryonic dorsal spinal cord. The spinal cord is derived from the posterior neuroectoderm as a result of both posteriorizing signals, such as retinoic acid (RA) (Diez del Corral et al., 2003; Molotkova et al., 2005), and regional identity cues, provided by the HOX genes (Forlani et al., 2003). The dorsal-most spinal cord is patterned most notably by the bone morphogenetic protein (BMP) family, secreted by the roof plate (RP) at the dorsal midline (Andrews et al., 2017; Hazen et al., 2012; Le Dreau and Marti, 2013; Liem et al., 1997; Yamauchi et al., 2008). RP-derived BMPs direct dorsal spinal progenitors toward three populations of dorsal sensory INs; the LHX2$^+$ dI1s (Liem et al., 1997), LHX1/5$^+$ PAX2$^-$ dI2s (Caspary and Anderson, 2003), and Isl1/2$^+$ TXL3$^+$ dI3s (Tsuchida et al., 1994). These neuronal populations fail to develop in mice lacking key type I BMP receptors (Wine-Lee et al., 2004) or if the RP is ablated *in vivo* (Lee et al., 2000).

This developmental paradigm suggested that the combinatorial action of RA and BMP4 will caudalize and dorsalize hESC-derived neural progenitors toward dorsal sensory INs, in a manner analogous to the protocols for generating stem cell-derived spinal MNs. However, dorsal sensory INs develop over a different timeline than MNs (Andrews et al., 2017; Le Dreau and Marti, 2012) and it has remained unresolved whether hESC-derived spinal progenitors are equally competent to give rise to MNs and INs. We thus first characterized cell fate transitions during the early stages of hESC neuralization to determine the optimal time point to add BMP4. We thereby demonstrated that BMP4 directs hESCs toward dI1 and dI3 fates within a temporally restricted window that is different than that for spinal MNs. Unexpectedly, dI2s are observed in the RA control conditions and are suppressed after BMP4 addition. We further show that hESC-derived sensory INs express mature axonal markers of the spinal cord, suggesting they functionally mirror their endogenous counterparts. Finally, we established that this protocol directs human iPSCs to differentiate into dI1 and dI3s with comparable efficiency with hESCs. Thus, these two types of pluripotent stem cells can follow a similar developmental program to generate sensory INs. Taken together, this study paves the way for further understanding of the diseases of somatosensory system and designing cellular replacement therapies to regain somatosensation in SCI patients.

RESULTS

Characterizing the Timeline by which hESCs Lose Pluripotency and Enter the Neurogenic Lineage

We sought to generate *in-vitro*-derived dorsal spinal sensory INs by modifying the protocol used to generate spinal MNs (Wichterle and Peljto, 2008). In brief, this protocol directs hESCs toward MN fates in three steps: hESCs are first cultured in a neural differentiation medium (SaND medium) (Sareen et al., 2013), to direct them toward a neurogenic lineage. Second, hESCs are caudalized by the addition of RA (Figure 1A). Third, they are ventralized by the addition of a sonic hedgehog signaling agonist, such as purmorphamine, to specify spinal MN identity. We hypothesized that adding BMP4 protein, instead of purmorphamine, to the caudalized hESCs would generate BMP-dependent dorsal sensory INs, given the role of the BMPs directing dorsal spinal fate (Andrews et al., 2017; Liem et al., 1997). However, dorsal sensory INs develop along a different timeline from ventral MNs *in vivo* (Andrews et al., 2017; Le Dreau and Marti, 2012). Thus, we first assessed the timing by which hESCs enter the neurogenic and spinal progenitor program, to determine the optimal day on which to add growth factors.

We assessed when hESCs lose pluripotency and enter the neurogenic program by examining the expression

Figure 1. Timeline for the Onset of the Neurogenic Program in hESCs

(A) Timeline and methodological details of the differentiation protocol to derive dorsal spinal sensory INs from hESCs.

(B–G) hESCs were collected for IHC and RT-qPCR analyses at day 0, 2 (B and E), 4 (C and F), and 6 (D and G) using antibodies against NANOG (red), PAX6 (green, B–D) SOX1 (green, E–G), SOX2 (blue, B–D), and DAPI (blue, E–G).

(H) hESCs rapidly exit the pluripotent state. The number of NANOG$^+$ cells ($p < 0.0001$) and levels of *NANOG* transcript (0, $p < 0.0001$) decline by day 2 (B′) and are undetectable by day 4 (C′ and D′).

(I and J) Concomitantly hESCs enter a neurogenic state: *SOX2* transcript and SOX2 protein levels remain constant (I), while *SOX1* mRNA (J, $p < 0.005$) and SOX1 protein (J, $p < 0.0001$) are induced by day 2. *SOX1* expression starts to decline at day 4 (J), with the number of SOX1$^+$ cells decreasing at day 6. By day 6, the remaining SOX1$^+$ cells are found clustered together (G). *PAX6* starts to be expressed at day 4 ($p < 0.01$) (C‴–D‴ and K).

Two biological replicates were performed, with at least five fields of cells quantified for every IHC condition. The number of cells is expressed as a percentage of the total number of DAPI$^+$ cells. Probability of similarity **$p < 0.005$, ***$p < 0.0005$. Scale bar, 100 μm.

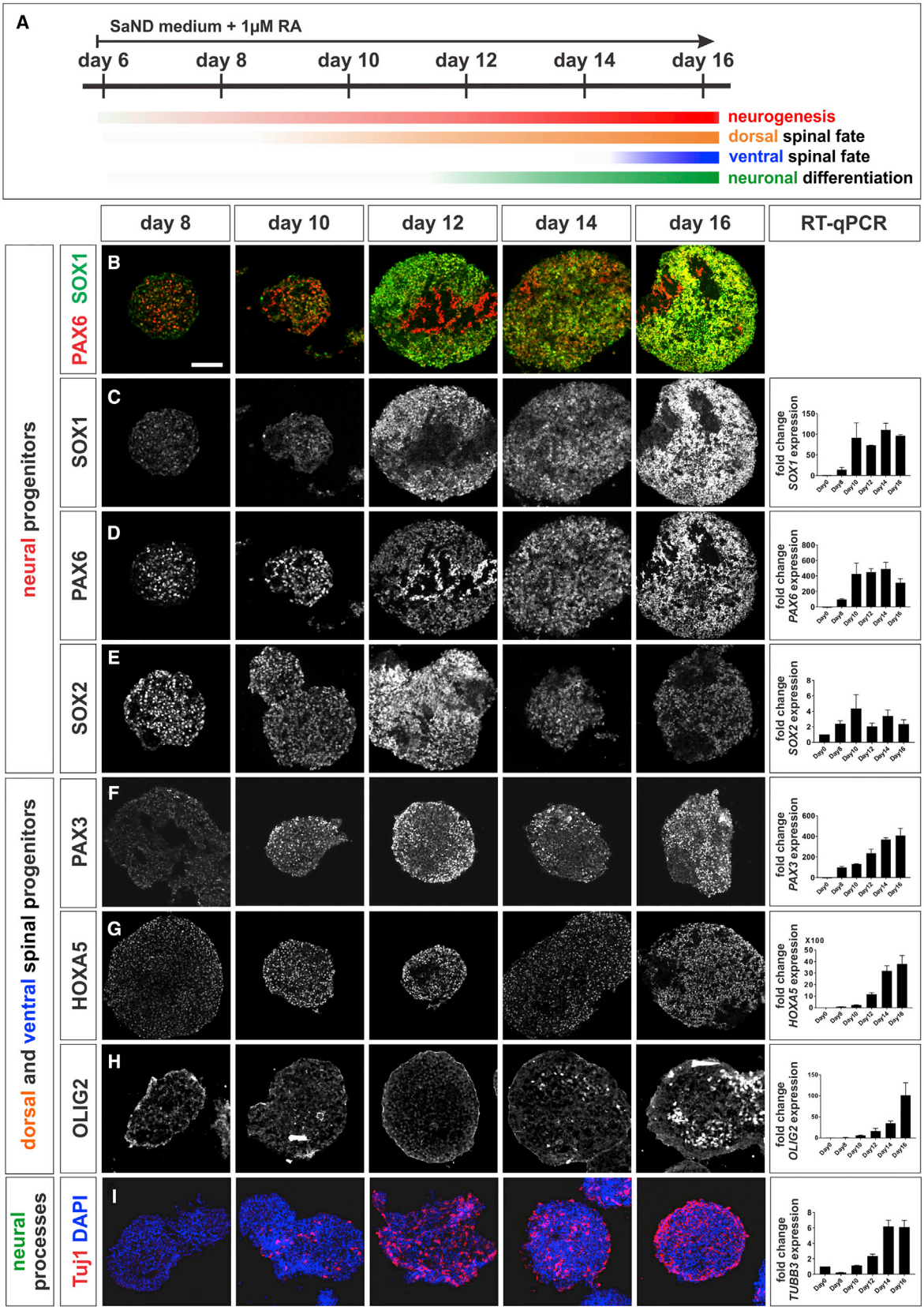

(legend on next page)

levels and distribution of NANOG, SOX2, PAX6, and SOX1 during the first 6 days of two-dimensional culture in SaND medium. NANOG is present specifically in undifferentiated precursors (Mitsui et al., 2003), SOX2 labels both pluripotent and neuroectodermal cells (Bylund et al., 2003; Ellis et al., 2004; Graham et al., 2003), while PAX6 and SOX1 are pan neuroectodermal markers (Pevny et al., 1998; Walther and Gruss, 1991). The number of NANOG$^+$ cells (Figures 1B′–1D′ and 1H) and *NANOG* mRNA levels (Figure 1H) decline rapidly by day 2 of the protocol and are undetectable by day 4, suggesting hESCs rapidly exit the pluripotent state (Figure 1A). In contrast, the number of SOX2$^+$ cells (Figures 1B″–1D″ and 1I) and level of *SOX2* transcript (Figure 1I) remained stable during this 6-day period, indicating that hESCs start to upregulate the neurogenic program by day 2. This hypothesis was supported by the observation that *PAX6* RNA and PAX6 protein are induced by day 4 and increase by day 6 (Figures 1B‴–1D‴ and 1J). Similarly, *SOX1* expression initiated in hESCs by day 2 (Figures 1E–1G and 1K). However, *SOX1* expression subsequently declines, with the numbers of SOX1$^+$ cells peaking at day 4, and an ~5-fold decrease in *SOX1* mRNA by day 6 (Figure 1K). Together, this analysis suggests that culturing hESCs in SaND medium permits them to initiate neurogenesis. However, this state is not sustained past day 6, suggesting that RA, a pro-neuralization factor (Engberg et al., 2010; Tonge and Andrews, 2010), should be added to the cultures at this time point.

RA Directs hESCs toward Spinal Progenitors with Mixed Identities

We next assessed the effect of adding RA at day 6 on neuroepithelial fates in the hESC cultures. hESCs were permitted to form embryoid bodies (EBs) in SaND medium supplemented with 1 μM RA. The levels of both *SOX1* and *PAX6* mRNAs markedly increase, reaching a plateau by day 10 (i.e., after 4 days of RA exposure) (Figures 2B–2D). *SOX2* mRNA and SOX2 protein levels also modestly increase until day 12 but decline thereafter, suggesting an erosion of the progenitor state (Figure 2E). The decline in SOX2 levels correlates with the onset of neuronal differentiation. Tuj1, an antibody that labels neural processes (Menezes and Luskin, 1994), starts to decorate human EBs (hEBs) at day 10 and becomes robust by day 14 (Figure 2I), suggesting that progenitors have begun to differentiate into post-mitotic neurons.

We also determined the time frame over which RA induces hEBs toward spinal progenitor fates by analyzing *HOX*, *PAX3*, and *OLIG2* expression. The HOX profile indicates axial level (Philippidou and Dasen, 2013), PAX3 is broadly present in dorsal spinal progenitors (Mansouri and Gruss, 1998), and OLIG2 marks the MN progenitor (pMN) domain (Novitch et al., 2001). A 2-day exposure to RA (day 8) was sufficient to induce *HOXA5*, with robust numbers of HOXA5$^+$ cells observed by day 10 (Figure 2G). There were markedly more modest levels of *HOXA9* and *HOXA11*, with no expression of either *HOXD11* or *HOXA13* (Figures S1D and S1E), demonstrating that the hEBs have generally adopted a rostral cervical spinal identity. However, the EBs contain both dorsal and ventral spinal progenitors: *PAX3* mRNA and PAX3 protein are present at high levels by day 8 (Figure 2F), while *OLIG2* expression starts at day 10, but is not robust until day 16, when many OLIG2$^+$ cells are also observed (Figure 2H). Thus, there are two phases of RA action: an early phase (day 6–10) where RA induces dorsal spinal progenitors, and a later phase (after day 12), when prolonged exposure to RA results in ventral spinal progenitors and the onset of neuronal differentiation.

BMP4 Induces hEBs toward Dorsal Sensory IN Fates within a Specific Temporal Window

We next determined the consequence of adding BMP4 in addition to RA to the hEB cultures. Previous studies (Andrews et al., 2017; Chizhikov and Millen, 2004; Le Dreau and Marti, 2013) have shown that BMP4 is sufficient to direct ectopic Lhx2$^+$ dI1, Lhx1/5$^+$ Pax2$^-$ dI2 and Isl1$^+$ Tlx3$^+$ dI3 cells in embryonic chicken spinal cords. We verified that these markers of dorsal IN identity are evolutionarily conserved in primates, by assessing the distribution of Lhx2 and Isl1 in day 28 Rhesus macaque embryos, a stage equivalent to embryonic (E) stage 11.5

Figure 2. Retinoic Acid Induces Dorsal Spinal Fate in the hESCs

(A) At day 6, the neuralized hESCs were dissociated and allowed to form EBs in SaND medium, supplemented with 1 μM RA. Samples were taken at day 6, 8, 10, 12, 14, and 16 for IHC and RT-qPCR analysis to characterize the early effects of RA on EB identity.

(B–E) RA promotes neural identity: *SOX1* (B and C) and *PAX6* (B and D) expression increases markedly by day 12. *SOX2* starts to decline by day 12, suggesting the onset of neuronal differentiation (E).

(F–H) RA rapidly caudalizes EBs, resulting in a HOXA5$^+$ spinal identity from day 10 (G). EBs also show mixed identities, RA promotes both PAX3$^+$ dorsal fates by day 8 (F) and OLIG2$^+$ ventral fates by day 14 (H).

(I) Longer RA incubation induces neural differentiation, marked by Tuj1 expression in EBs (compare quantification on day 10 and day 12, $p < 0.009$).

Two biological replicates were performed. Scale bar, 100 μm.

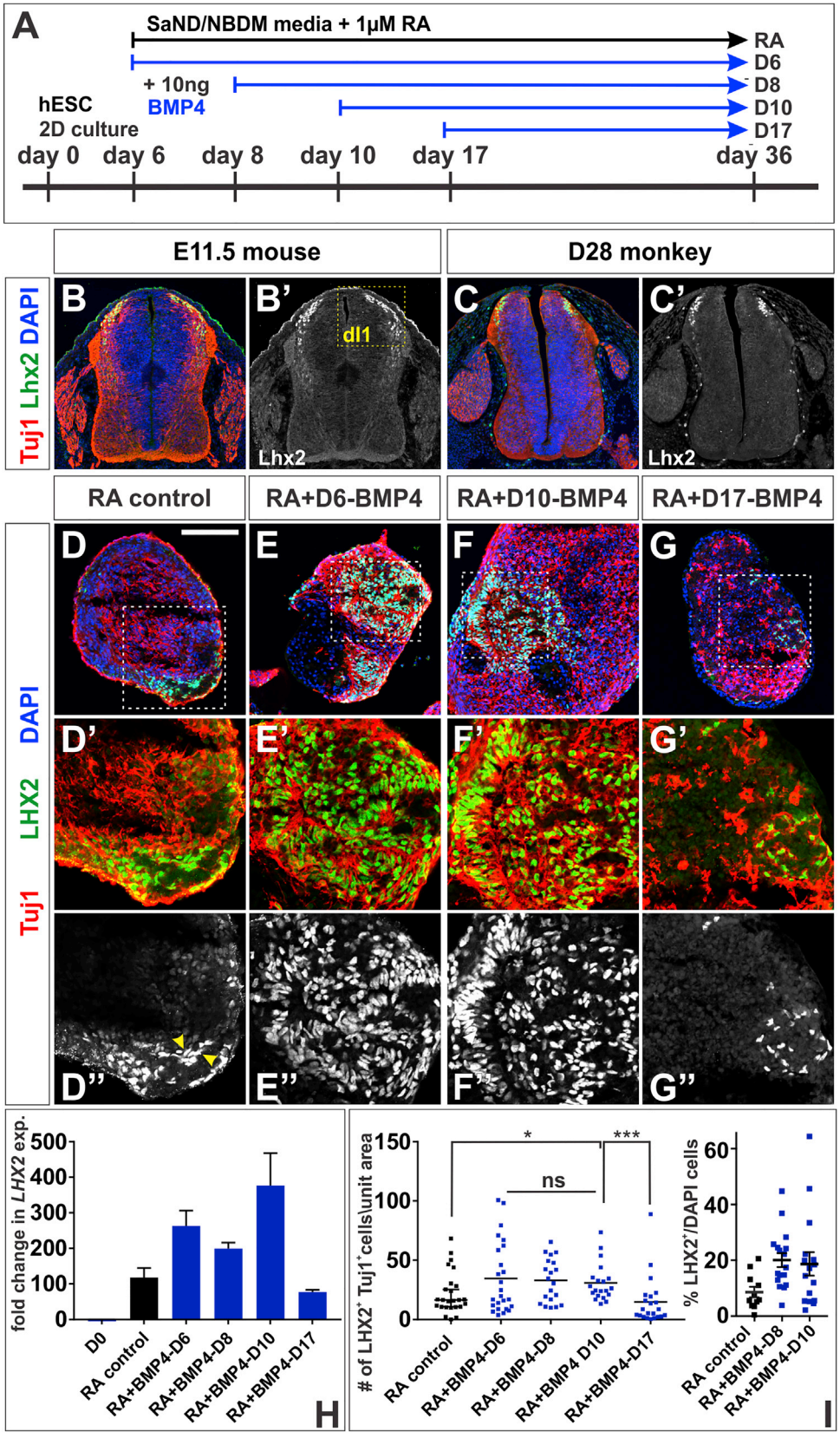

(legend on next page)

mouse (Clark et al., 2017). Strikingly, the distribution of Lhx2 and Isl1 were similar in primates and rodents (Figures 3B, 3C, 4A, and 4B).

We hypothesized that the addition of BMP4 to hEBs exposed to a short period of RA (i.e., from day 6 to 10 before either ventralization or neuronal differentiation) would be the condition most likely to induce dorsal sensory INs. BMP4 (10 ng/mL) was added to the RA-treated hEBs at day 6, 8, 10, and 17 (Figure 3A). The hEBs were cultured until day 36 and then analyzed for the distribution and level of SOX2, pHISTONEH3, LHX2, LHX1/5, ISL1, and PAX2. The EBs are still differentiating at day 36, with 1%–2% of the cells in mitosis (Figures S2A′–S2D′ and S2J), and up to ~50% of the cells in the EBs continuing to express SOX2 (Figures S2A–S2D and S2I).

Consistent with our hypothesis, the addition of BMP4 on any day during the RA-early phase (i.e., BMP4-D6, BMP4-D8, and BMP4-D10) resulted in an up to 3-fold increase in the expression of *LHX2* and a >2-fold increase in the number of LHX2$^+$ Tuj1$^+$ dI1s (Figures 3E, 3F, 3H, and 3I, see Figures S3A–S3C for biological replicates) compared with RA control (Figures 3D, 3H, and 3I). Measuring the number of LHX2$^+$/DAPI$^+$ nuclei within EBs suggested an average dI1 differentiation efficiency of ~20% (Figure 3I, summarized in Table S3). In contrast, there was no significant increase in either *LHX2* expression or the number of LHX2$^+$ Tuj1$^+$ cells, when BMP4 was added during the RA-late phase (i.e., BMP4-D17) (Figures 3G, 3H, and 3I).

Similarly, the addition of BMP4 to hEBs during the RA-early phase led to 3-fold increased *ISL1* expression and up to 3-fold more ISL1$^+$ Tuj1$^+$ cells (Figures 4D, 4E, 4G, and 4H, see Figures S3D–S3F for biological replicates) compared with RA control (Figures 4C, 4G, and 4H). These ISL1$^+$ cells could be co-labeled with TLX3, which marks a subset of dI3s (Muller et al., 2005) (Figures S4B, S4C, and S4E–S4G), but not with HB9, a marker of spinal MNs (Arber et al., 1999) (Figures S4D and S4H), verifying their identity as dorsal dI3s. The average dI3 differentiation efficiency is ~15% (Figure 4H, Table S3). There was again no significant increase in either *ISL1* expression or the number of ISL1$^+$ Tuj1$^+$ cells, when BMP4 was added during the RA-late phase (Figures 4F, 4G, and 4H).

Surprisingly, we did not find a condition where the addition of RA + BMP4 was able to induce dI2s, as was observed in chicken embryos *in vivo* (Andrews et al., 2017). Rather we found that LHX1/5$^+$ PAX2$^-$ dI2s are present in the RA condition (Figures S2E and S2K–S2N), with an average dI2 differentiation efficiency of ~15% (Figure S2K and Table S3). In contrast, BMP4 appears to suppress the dI2 fate: after the addition of RA + BMP4 there is a 10-fold decrease in *LHX1* or *LHX5* expression and at least a 5-fold decrease in the number of LHX1/5$^+$ PAX2$^-$ cells (Figures S2F, S2G, and S2K–S2N).

Taken together, these data suggest that neural progenitors are most competent to generate BMP4-derived dorsal sensory INs after a brief exposure to RA. Supporting this model, we find that *ATOH1* and *ASCL1* expression is increased in hEBs after early BMP4 addition (Figures 5D and 5E). *ATOH1* (also known as Math1) and *ASCL1* (also known as Mash1) expression defines the progenitor state for the dI1s (i.e., the dorsal progenitor [dP] 1 domain) (Figure 5B (Helms and Johnson, 1998)) and dI3s (i.e., dP3) (Figure 5C, Helms et al., 2005), respectively. This competence window has closed by 11 days (day 17) of RA treatment.

Differentiated hEBs Exhibit Mature Axonal Markers of the Dorsal Spinal Cord

We next started to assess whether our directed differentiation protocol generates dorsal INs with the relevant functional characteristics, by analyzing day 36 hEBs for the presence of ROBO3 and DCC. DCC (Keino-Masu et al., 1996) and ROBO3 (Sabatier et al., 2004) are transmembrane receptors required for the guidance of spinal commissural axons. The presence of ROBO3 and DCC in the spinal cord is evolutionarily conserved between rodents and primates; however, there may be

Figure 3. BMP4 Directs hESCs toward Proprioceptive-dI1 Sensory Interneurons

(A) BMP4 was added to neuralized EBs at day 6 (BMP4-D6), 8 (BMP4-D8), 10 (BMP4-D10), or 17 (BMP4-D17). EBs were collected at day 36 for IHC and RT-qPCR analyses to characterize the effects of BMP4 on dorsal neural identity.

(B and C) Transverse sections of E11.5 mouse lumbar (B) and day 28 monkey thoracic (C) embryonic spinal cord labeled with antibodies against β-III tubulin (red, Tuj1) and Lhx2 (green). The Lhx2$^+$ Tuj1$^+$proprioceptive dI1s originate in the dorsal-most spinal cord (B, box, B′).

(D–I) The addition of BMP4 at day 6 (E), 8 or 10 (F) resulted in elevated *LHX2* expression (H) and significantly increased production of LHX2$^+$ Tuj$^+$ dI1s (E″, F″, and I) compared with RA controls (D″ and I; probability similar to RA control: $p = 0.25$, BMP4-D6; $p < 0.043$, BMP4-D8; $p < 0.016$, BMP4-D10); ~20% of the BMP4-treated cells are LHX2$^+$ (I). However, this effect is lost if BMP4 is added at day 17 (G, H, and I; probability similar to RA control, $p = 0.20$). There is no significance difference in *LHX2* expression levels or numbers of LHX2$^+$ Tuj$^+$ dI1s among the BMP4-D6, BMP4-D8, and BMP4-D10 conditions (L, $p = 0.77$, BMP4-D6 versus BMP4-D8 versus BMP4-D10, one-way ANOVA). Note that in the RA condition, not all LHX2$^+$ cells are Tuj1$^+$ (arrows, D″). The region in the white dashed box in (D)–(G) is shown at higher magnification in (D′)–(G′) and (D″)–(G″).

Probability of similarity $^*p < 0.05$, $^{***}p < 0.0005$. Six biological replicates were performed, with 20–25 EBs quantified. The number of cells was normalized to the area of the EB and then scaled according to a unit area (10,000 μm^2). Scale bar, 100 μm.

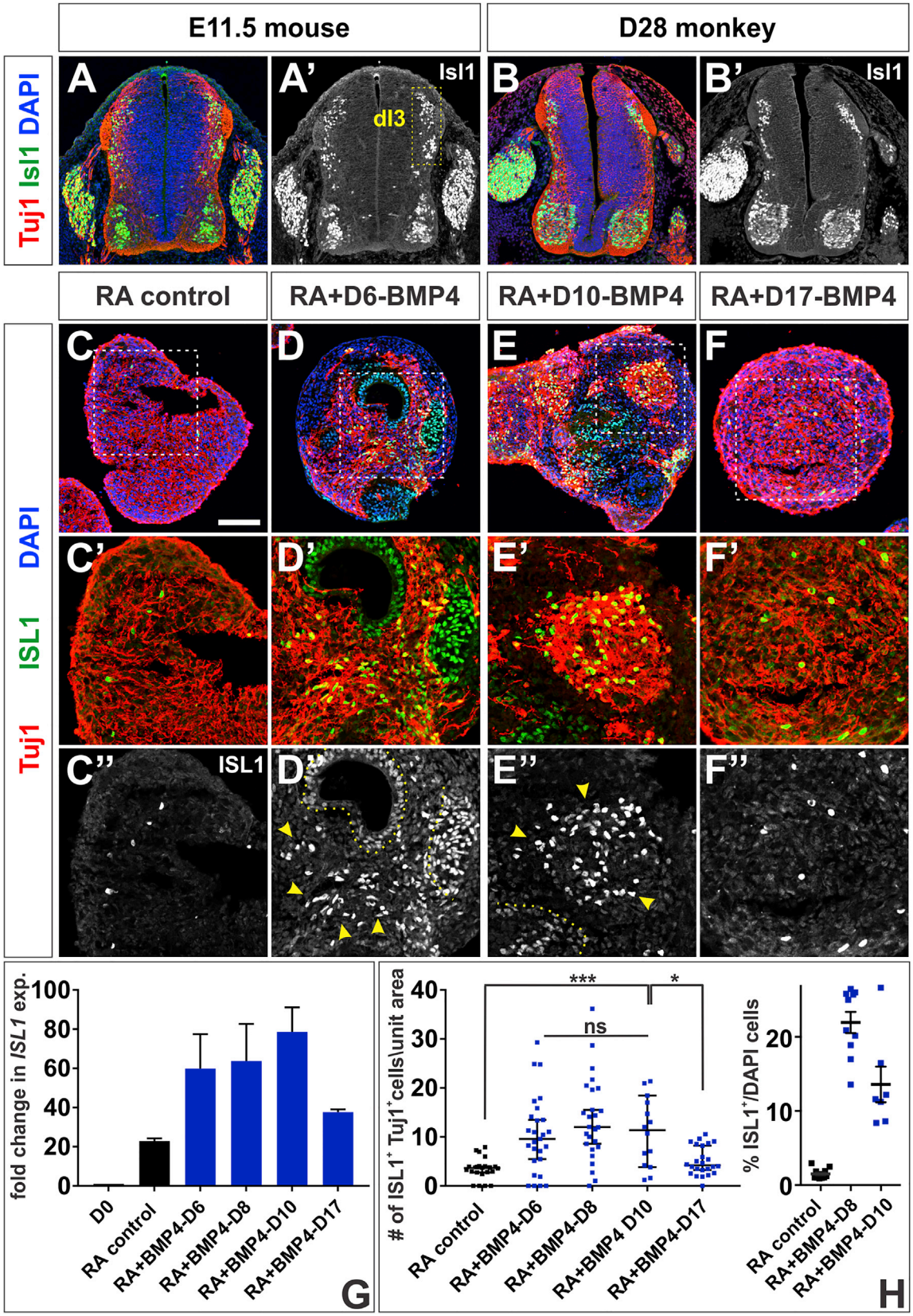

(legend on next page)

species-specific differences. While both Dcc and Robo3 are present broadly in axons crossing the ventral commissure in E11.5 mouse embryos (Figures 6A and 6C), Dcc and Robo3 have sparser distribution in day 28 monkey spinal cords. Dcc is generally present on axons in the dorsal spinal cord (arrows, Figure 6B′), while Robo3 is present on the soma of neurons in the intermediate spinal cord (arrows, Figure 6D′) as well as pioneering commissural axons in the ventral spinal cord.

Both DCC and ROBO3 are present in RA control and RA + BMP4-treated EBs by day 36. However, the DCC^{+} ROBO3^{low} expression profile in the BMP4-D6 and BMP4-D10 hEBs (Figures 6F′, 6G′, 6J′, and 6K′) was distinct from the DCC^{+} ROBO3^{high} profile (Figures 6E′, 6H′, 6I′, and 6L′) observed in the RA control and BMP4-D17 condition. These profiles are consistent with the BMP4-D6 and BMP4-D10 conditions primarily inducing the dorsal-most dI1 spinal identity, while the RA and BMP4-D17 condition results in more intermediate dorsal identities. Thus, these hESC-derived dorsal INs have the expected complement of guidance receptors, consistent with the hypothesis that they are maturing into functional dorsal sensory neurons.

BMP4 Can Direct Human iPSCs toward dI1s and dI3s Fates

Finally, we assessed whether our protocol can be used to direct patient-derived iPSCs toward the dI1 and dI3 fates. BMP4 was added to iPSCs at day 10, and EBs collected at day 36. As observed for hESCs, we found a 4-fold increase in *LHX2* expression (Figure 7C) and a 2-fold increase in the number of LHX2^{+} Tuj1^{+} dI1s (Figures 7B′ and 7D) in the BMP4-D10 treated hEBs compared with RA control (Figure 7A′). We also observed a 2.5-fold increase in *ISL1* expression (Figure 7G) and a 2-fold increase in the number of ISL1^{+} Tuj1^{+} dI3s (Figures 7F′ and 7H) in the BMP4-D10-treated hEBs compared with RA control (Figure 7E′). Side-by-side differentiation procedures suggested that hESCs and iPSCs generated dI1 and dI3 sensory INs to comparable extents (Figures 7C, 7D, 7G, and 7H). Thus, this protocol is capable of deriving patient-specific sensory IN populations.

DISCUSSION

Human PSC technologies can generate the unlimited supply of cells needed to facilitate both cellular replacement therapies, and an understanding of the molecular details underlying human diseases. To date, significant progress has been made deriving spinal MNs from hESCs and iPSCs that would permit the recovery of coordinated movement (Harper et al., 2004; Miles et al., 2004; Wichterle et al., 2002). However, to regain full function, a second critical class of neurons is needed: the dorsal sensory INs that integrate and relay somatosensory information from the periphery to the brain. Here, we report on the development of a robust protocol that permits the derivation of spinal sensory INs from hESCs and hiPSCs by the sequential addition of RA ± BMP4.

Establishing the Timeline over which hESCs Are Neuralized and Become Differentially Competent

We used the well-defined spinal MN-directed differentiation protocol as our starting point in our studies, hypothesizing that these hESC-derived neural progenitors are competent to become multiple post-mitotic neuronal identities. We first characterized hESCs as they acquire neural and spinal identity. The onset of hESC neuroectodermal identity is marked by a rapid decline in pluripotency and the upregulation of SOX1 and then PAX6 (Figure 1). This temporal order is similar to that observed during mouse neuroectodermal development (Pevny et al., 1998; Suter et al., 2009), suggesting that we have recapitulated a development program conserved between rodents and humans. Previous hESC neuralization protocols have reported an inverted temporal order of *SOX1* and *PAX6* expression as hESCs neuralize (Gerrard et al., 2005; Wu et al., 2010).

Figure 4. BMP4 Directs hESCs toward Mechanosensory-dI3 Interneurons

(A and B) Transverse sections of E11.5 mouse lumbar (A) and day 28 Rhesus macaque thoracic (B) embryonic spinal cord labeled with antibodies against β-III tubulin (red, Tuj1) and Isl1 (green). The Isl1^{+} Tuj1^{+} mechanosensory dI3 cells are present in the intermediate spinal cord (A, box, A′).

(C–H) Addition of BMP4 at day 6 (D), 8 or 10 (E) resulted in elevated *ISL1* expression (G) and significantly increased production of ISL1^{+} Tuj^{+} dI3s (arrowheads, D″, E″, quantified in H) compared with RA controls (C″ and H; probability similar to RA control: $p < 0.004$, BMP4-D6; $p < 0.0001$, BMP4-D8; $p < 0.0008$, BMP4-D10); ∼15% of the BMP4-treated cells are ISL1^{+} (H). However, this effect is lost when BMP4 is added at day 17 (F″, G, and H, probability similar to RA control, $p > 0.09$). There is no significant difference in *ISL1* levels or numbers of ISL1^{+} Tuj^{+} dI3s in the BMP4-D6, BMP4-D8 and BMP4-D10 conditions (L, BMP4-D6 versus BMP4-D8 versus BMP4-D10, $p > 0.37$, one-way ANOVA). Note that not all ISL1^{+} cells are Tuj1^{+} (dotted lines, D″, and E″). The region in the white dashed box in (C)–(F) is shown in higher magnification in (C′)–(F′) and (C″)–(F″).

Probability of similarity *$p < 0.05$, ***$p < 0.0005$. Six biological replicates were performed with 14–27 EBs quantified. The number of cells was normalized and then scaled according to a unit area (10,000 μm^2). Scale bar, 100 μm.

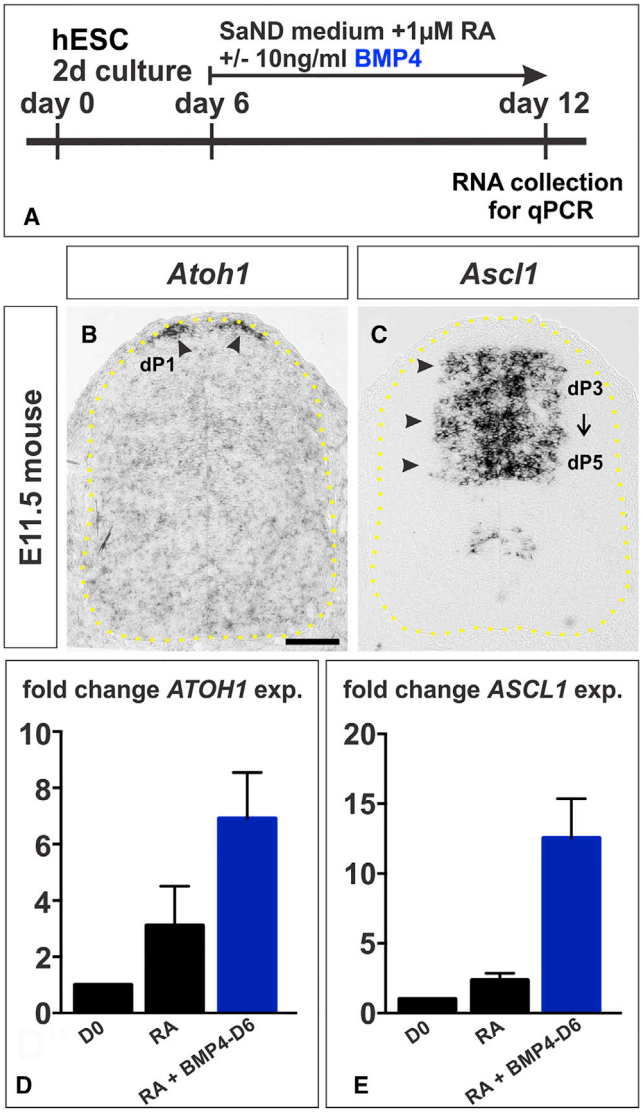

Figure 5. BMP4 Directs hESCs toward Dorsal Neural Progenitor Identities

(A) To assess the acquisition of dorsal progenitor identity, EBs were cultured for 12 days, with BMP4 added at day 6.

(B and C) In the mouse spinal cord (indicated by yellow dotted lines, B and C), the dP1 and dP3-5 domains express *Atoh1* (arrowheads, B) and *Ascl1* (arrowheads, C), respectively, in the E11.5 mouse embryo. The dP1 cells give rise to Lhx2$^+$ dI1s while Isl1$^+$ dI3s emerge from the dP3-5 population.

(D and E) BMP4 addition increases *ATOH1* levels by >2-fold (D, probability of similarity with RA control, $p < 0.038$) and *ASCL1* levels by >5-fold (E, $p < 0.024$).

Four biological replicates were performed. Scale bar, 100 μm.

This discrepancy may arise from the way in which neuroectodermal identity was achieved: the previous studies used noggin to facilitate neuralization by blocking BMP signaling, and basic fibroblast growth factor (bFGF) to maintain the proliferation capacity of the neural progenitors. However, we neuralized hESCs using the B27/N2 supplements present in SaND medium, which may result in hESCs initiating neurogenesis in a manner closer to the endogenous process.

We found that RA should be added at day 6 to maintain a stable SOX1$^+$ PAX6$^+$ neurectodermal identity. By day 12, these cells had a HOX profile most consistent with a HOXA5$^+$ cervical spinal identity (Figure 2G), with a small component from the HOXA9$^+$ thoracic level (Figure S1). There is little to no *HOXD11* or *HOXA13* expression (Figures S1D and S1E), suggesting that the cells do not have a lower lumbar-sacral identity. The HOX profile may depend on the concentration and duration of RA exposure, as well as the presence of other caudalizing factors. Studies using a combination of RA and FGF2 have generated spinal neurons with a more posterior HOX gene profile (Li et al., 2005).

The Competence State of hESC-Derived Spinal Progenitors Changes over Time

We assessed whether hESC-derived spinal progenitors are simultaneously competent to give rise to either MNs or INs, or whether the competence state changes over time. We found that that the addition of RA induces PAX3$^+$ dorsal progenitors by day 8, while OLIG2$^+$ ventral progenitors arise later, by day 14. Consistent with the hypothesis that progenitor competence state changes over time, early RA-treated spinal progenitors are most competent to give rise to dI1 and dI3s in response to BMP4. This competence for dorsalization is lost by day 17, the day at which purmorphamine is typically added to hESC-derived spinal progenitors to direct them toward MN fates (Sareen et al., 2013). The molecular basis for these different competence states remains unresolved. Longer RA incubation may alter the transcriptome of the hESCs-derived spinal progenitors, rendering them unresponsive to BMP4.

Unexpectedly, we were unable to derive BMP4-dependent dI2s; these cells were only observed in the RA condition. In the developing spinal cord, BMP signaling is both necessary and sufficient to specify the dI2 fate (Andrews et al., 2017; Wine-Lee et al., 2004). However, our recent experiments have suggested that dorsal progenitors are not equivalently competent to respond to BMP4 (Andrews et al., 2017). We have found that BMP4 is both a patterning and differentiation signal for dI1/dI3s, able to specify dP1/dP3 progenitors and then reiteratively direct them to form dI1s and dI3s. In contrast, BMP4 is specifically a differentiation cue for dI2s: it directs Ngn2$^+$ progenitors to differentiate into dI2s. Taken together, our studies suggest adding BMP4 to hESCs directs them first toward a dP1/dP3 progenitor state; the

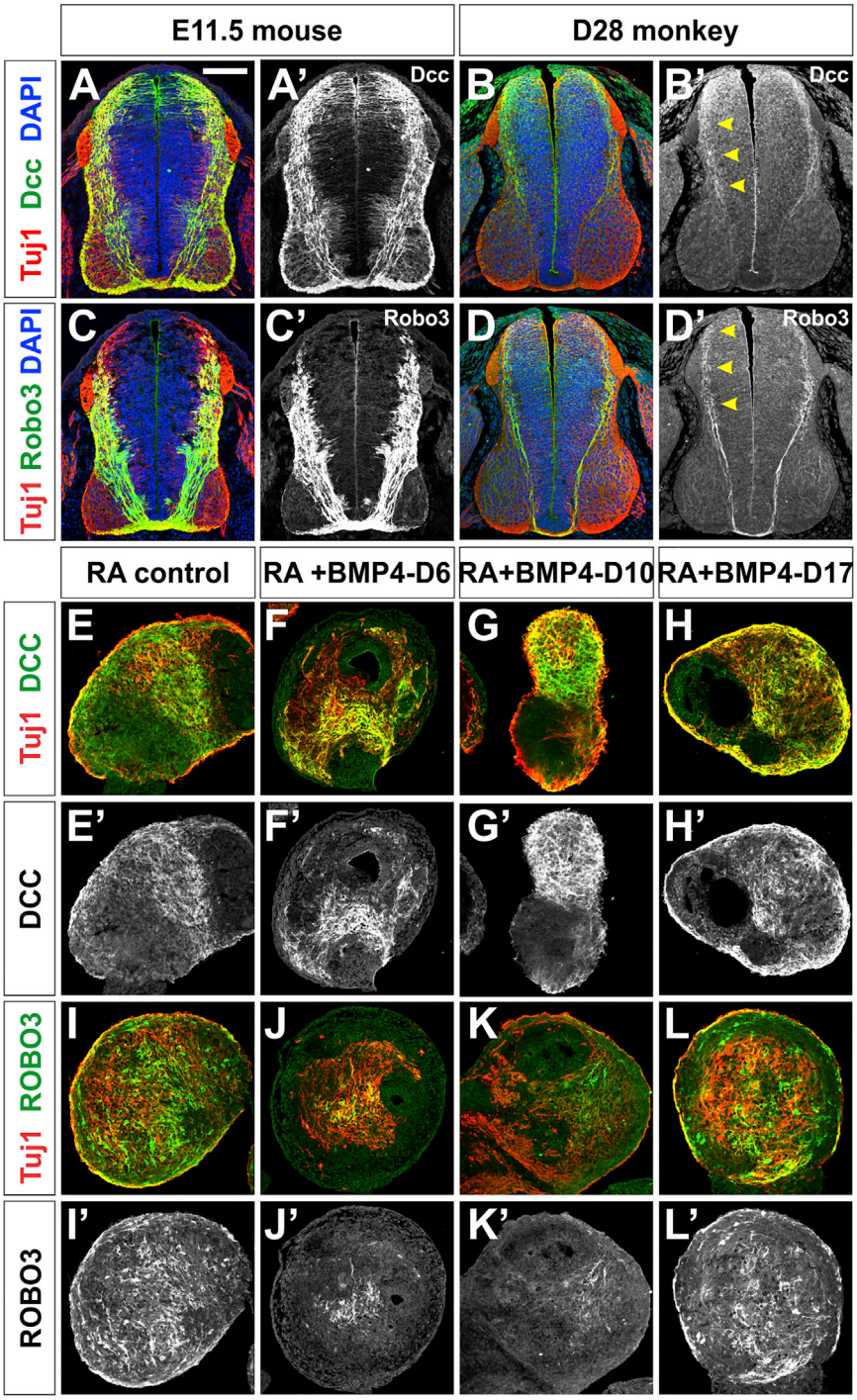

Figure 6. hESC-Derived EBs Express DCC and ROBO3, Two Markers of Spinal Commissural Axons

(A–D) Transverse sections of E11.5 mouse lumbar (A and C) and day 28 monkey thoracic (B and D) spinal cord labeled with antibodies against Tuj1 (red), Dcc (green, A and B), Robo3 (green, C and D) and DAPI (blue). Dcc and Robo3 are broadly present on mouse commissural (A′ and C′) axons. In contrast, Robo3 is present in a sparser population of monkey commissural axons arising from neurons in the intermediate spinal cord (arrowheads, D′). Dcc decorates the axons of dorsally derived commissural neurons (arrowheads, B′).

(E–H) Day 36 EBs treated with RA, RA + BMP4-D6, RA + BMP4-D10 and RA + BMP4-D17, were labeled with antibodies against Tuj1 (red), DCC (green, E–H) and ROBO3 (green, I–L). Numerous DCC^+ $Tuj1^+$ and $ROBO3^+$ $Tuj1^+$ axons were present in the control and experimental EBs. The ROBO3 and DCC stainings are more extensive in the RA control (E′ and I′) and BMP4-D17 EBs (H′ and L′), compared with BMP4-D6 (F′ and J′) and BMP4-D10 (G′ and K′) EBs, consistent with these conditions generating cells with distinct dorsal identities.

Scale bar, 100 μm.

continued presence of BMP4 then acts as pro-dI1/dI3 signal. The dP2 progenitor state is suppressed, thereby generating no BMP4-dependent dI2s. In contrast, adding RA to hESCs appears to generate multiple dorsal progenitor populations, which in turn results in mixed dorsal IN identities, including some dI1s, the more robust production of dI2s, as well as more intermediate dorsal INs, such as dI4s (Table S3).

Future studies will identify the mechanism by which BMP4 produces both dI1s and dI3s. Does BMP4 induce a common dP1/dI3 progenitor state? Or do fluctuations in BMP signaling specify distinct dP1 and dP3 populations?

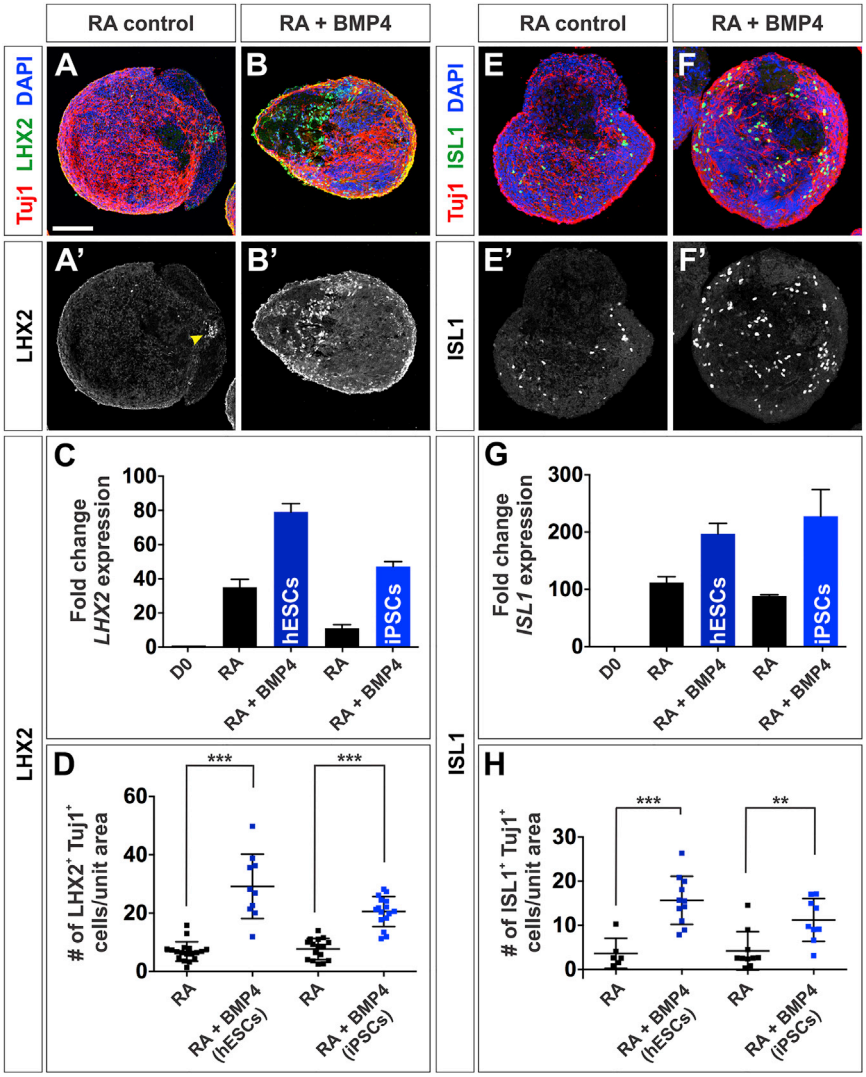

Figure 7. BMP4 Also Directs iPSCs toward a dI1s and dI3 Identity

(A–H) Day 36 EBs, derived from iPSCs treated with RA and RA + BMP4-D10, were either processed for RT-qPCR or labeled with antibodies against Tuj1 (red), LHX2 (green, A and B), ISL1 (green, E and F), and DAPI (blue).

(A–D) The BMP4-D10 condition resulted in a significant increase in *LHX2* mRNA and number of LHX2$^+$ Tuj1$^+$ dI1s in both hESC-derived EBs (C, probability similarity with RA control $p < 0.023$; D, $p < 0.0001$) and iPSC-derived EBs (C, $p < 0.0096$; B′ and D, $p < 0.0001$) compared with RA control (arrow, A′ and D).

(E–H) The BMP4-D10 condition also resulted in a significant increase in *ISL1* expression in hESCs-EBs (G, $p < 0.016$) and iPSC-EBs (G, $p < 0.04$) and the number of ISL1$^+$ Tuj1$^+$ dI3s (hESCs-EBs: H, $p < 0.0005$; iPSC-EBs: F′ and H, $p < 0.0022$), compared with RA control (E′, G, and H).

Three biological replicates were performed. Probability of similarity: $^{**}p < 0.005$, $^{***}p < 0.0005$. Three biological replicates were performed with 10–18 EBs quantified. The number of cells was normalized and then scaled according to a unit area (10,000 μm^2). Scale bar, 100 μm.

We will also investigate how to deploy BMP signaling to improve the efficiency by which spinal progenitors are directed to become dI2s.

hESC-Derived Sensory INs May Functionally Mirror Their Endogenous Counterparts

The addition of BMP4 to the hESCs cultures led to ~35% of the cells in an hEB becoming dI1s and dI3s (Table S3). To start to address whether these neurons functionally resemble their endogenous counterparts, we assessed whether the hESC-derived human sensory INs express DCC and ROBO3, the guidance receptors required for growth of commissural axons toward the ventral midline (Sabatier et al., 2004; Varadarajan et al., 2017). DCC is present in hEBs at high levels as predicted from the distribution of Dcc in both mouse and monkey. However, the number of ROBO3$^+$ neurons was lower than we anticipated in the BMP4-directed hEBs compared with the RA control. Mouse Robo3 is present at high levels on commissural neurons and their axons throughout the dorsal and intermediate spinal cord (Sabatier et al., 2004; Varadarajan and Butler, 2017; Varadarajan et al., 2017). However, monkey Robo3 is primarily present on intermediate spinal neurons, and that the pioneering commissural axons appear to stem from this intermediate population (Figure 6D′). Thus, there may be species-specific differences in the complement of axonal guidance receptors present on dorsal neurons, and the timing by which sensory circuitry is established. The functional implications of this finding require further studies; however, one possibility is that DCC$^+$ ROBO3^{low} is the correct complement of axonal receptors for primate dI1 neurons. An alternative hypothesis is that the presence of BMP4 inhibits the maturation process of the spinal INs thereby reducing the ROBO3 levels.

In future studies, we will assess how closely the transcriptomic and electrophysiological profiles of hESC-derived sensory INs mirror neurons *in vivo*. Complicating this analysis, these properties have not yet been well defined for the endogenous sensory INs.

Clinical Implications of These Studies

For this protocol to be clinically relevant, it must also be applicable to patient-derived iPSCs. Previous studies have shown that differences in the epigenetic landscape can result in iPSC lines having varied differentiation efficiencies compared with hESCs (Hu et al., 2010). However, we found no noticeable difference between an iPSC and hESC line with respect to their ability to generate dI1s and dI3s. Thus, our protocol is robust and can be used to derive patient-specific sensory INs.

The present study completes the first step toward functionally re-building damaged spinal cords, by re-establishing the sensory connections that would allow an injured patient to perceive external stimuli. *In-vitro*-derived sensory INs can be used in drug testing platforms targeting diseased sensory INs as well as investigating the feasibility of using them in cellular replacement therapies. The ability to generate spinal INs *in vitro* will also accelerate studies examining the basis of debilitating spinal dysfunctions, such as congenital pain insensitivity and hereditary sensory and autonomic neuropathies (Nagasako et al., 2003).

EXPERIMENTAL PROCEDURES

Human ESC and iPSC Culture and Differentiation

H9 hESCs and iPSCs were obtained from the University of California, Los Angeles (UCLA) stem cell core and iPSC core at Cedars Sinai Medical Center, Los Angeles, respectively. Cells were maintained on Geltrex (Thermo Fisher Scientific)-coated plates in mTeSR1 medium (Stem Cell Technologies) at 37°C and in 5% CO_2 humidified incubators. Neural differentiation was initiated in two-dimensional culture by replacing mTeSR1 with SaND medium (IMDM + 2% B27-VitA + 1% N2 supplement; Thermo Fisher Scientific) (Sareen et al., 2013) for 6 days. After 6 days, hESCs or iPSCs were treated with Accutase (STEMCELL Technologies) for 2 min at 37°C, scraped off the plate using a glass pipette (Fisher Scientific) and collected by centrifugation at 1000 rpm in SaND medium. The cell pellet was resuspended in SaND medium + 1 μM all-*trans* RA (Sigma-Aldrich) + ROCK inhibitors (BioPioneer; SM-008), and the cells were permitted to form EBs in low-attachment 24-well plates (Corning). To induce dorsal IN differentiation (Figure 1A), 10 ng/mL BMP4 recombinant protein (Invitrogen, catalog no. PHC9534) was added at different time points between day 6 and day 17 (Figure 3A). At day 17, EBs were transferred to neural differentiation medium (NBDM) (Sareen et al., 2013) supplemented with 1 μM RA+ 10 ng/mL BMP4 for a further 8 days. To facilitate neuronal maturation, EBs were grown in neural maturation medium, consisting of Dulbecco's modified Eagle's medium⁄F12 and supplemented with B27 (2%), RA (1 μM), BMP4 (10 ng/mL), dibutyryl cyclic AMP (1 μM), ascorbic acid (200 ng/mL) until day 36 (Sareen et al., 2013). Control EBs were grown in 1 μM RA up until day 36.

Immunohistochemistry

Cells

Adherent hESC cultures were fixed with 4% paraformaldehyde (PFA) (Thermo Fisher Scientific, NC9658705) for 10 min at room temperature, and then washed with 1× PBS. EBs were fixed with 4% PFA for 30 min on ice, washed with 1× PBS, cryopreserved in a 30% sucrose solution, and thin sectioned to yield 12 μm sections. All cells were blocked (1% heat-inactivated horse serum + 0.1% Triton X-100 + 0.01% NaAz) for 1 hr and incubated with primary antibodies (see Table S1) overnight at 4°C. Species-appropriate cyanine 3, cyanine 5, and fluorescein-conjugated secondary antibodies (Jackson ImmunoResearch Laboratories) were used at room temperature for 2 hr.

Tissue Sections

Mouse tissue was processed for immunohistochemistry (IHC) as previously described (Varadarajan et al., 2017). Embryonic day 28 Rhesus macaque spinal cord was obtained through timed matings following Animal Care and Use Committee Approval (Clark et al., 2017). Embryos were fixed in 4% PFA, embedded in paraffin blocks, then cut to obtain 5-μm-thick transverse sections. For IHC staining, sections were deparaffinized and then rehydrated through a xylen/ethanol gradient. Sections were processed for immunohistochemistry as previously described (Clark et al., 2017). An antigen retrieval step using Tris-EDTA (10 mM Tris base, 1 mM EDTA solution, 0.05% Tween 20 [pH 9.0]) buffer at 95°C for 40 min was necessary. For nuclei staining, cells or sections were incubated with DAPI (1:1,000) in 1× PBS for 5 min and washed two times in 1× PBS. The sections were mounted in ProLong Gold mounting media (Thermo Fisher Scientific).

Imaging and Quantification

Images of adherent hESC cultures and EB sections were collected on an LSM800 confocal microscope using Carl Zeiss Zen Blue and processed using Adobe Photoshop CS6 software. The number of cells in adherent cultures were counted using the NIH ImageJ particle module, after modulating the intensity threshold in 8-bit images to capture the fluorescent cells. For the hESC counts (Figure 1) and differentiation efficiencies (Table S3), the number of cells is expressed as a percentage of the total number of $DAPI^+$ cells. For the EB cell counts (Figures 3, 4, and 7), the number of cells is divided by the area of the EB and then scaled according to a unit area (10,000 μm^2). Data points were pooled from multiple experiments.

Statistics

We performed each experiment 2–6 independent times (biological replicate), with 2–3 technical replicates (qPCR or IHC) for each biological replicate. Statistical analyses were performed using either a two-tailed Student's t test, if the data fit a normal distribution (Anderson-Darling test), or a Mann-Whitney test, if it did not. All data are represented as means ± SEM.

RNA Isolation and RT-qPCR Analysis

RNA was extracted using the RNeasy purification kit (QIAGEN, catalog no. 74104). cDNA was synthesized using Superscript IV (Thermo Fisher Scientific). RT-qPCR was always performed in triplicate using SYBR Green Master Mix (Roche) on a Roche RT-qPCR machine using gene-specific primers (Table S2). Sequences for primer pairs for HoxA11 (primer ID-84105266c2) and HoxA13 (primer ID-171906561c1) were obtained from PrimerBank-MGH-PGA (Spandidos et al., 2008, 2010; Wang and Seed, 2003). The Ct values for each gene were calculated by averaging two runs for each condition. Expression of the target gene was normalized with the expression of glyceraldehyde-3-phosphaste dehydrogenase (GAPDH) and fold change was calculated using the $2^{-\Delta\Delta Ct}$ method. We observed the same trends in all experiments, (i.e., the effect of RA versus RA + BMP4 in different biological replicates was always reproducible). However, the magnitude of the fold change in gene expression could vary markedly between biological replicates (Figure S3). Thus, each RT-PCR graph is taken from one of the biological replicates, and does not include statistics as required by the journal.

Ethical Statement

All hESC procedures were approved by the Embryonic Stem Cell Research Oversight committee at University of California, Los Angeles (UCLA). Monkey and mouse spinal cord tissue were obtained following approval from the UCLA Animal Care and Use Committee.

SUPPLEMENTAL INFORMATION

Supplemental Information includes four figures and three tables and can be found with this article online at https://doi.org/10.1016/j.stemcr.2017.12.012.

AUTHOR CONTRIBUTIONS

S.G., D.S., C.M., and S.H. performed the experiments. E.S. and A.C. provided tissue reagents. S.J.B., S.G., and D.S. conceived and designed the experiments. S.G. and S.J.B. wrote the manuscript.

ACKNOWLEDGMENTS

We are most grateful to Clive Svendsen and Ben Novitch for reagents. We would also like to thank Ben Novitch, as well as members of the Butler laboratory, for invaluable discussions and comments on the manuscript. The rhesus macaque tissues in this project were funded by support from the Oregon National Primate Research Center (OD11092). This work was supported by fellowships from the California Institute for Regenerative Medicine (CIRM) Bridges to Research program (TB1-01183) for S.H. and grants from CIRM (RB5-07320), the NIH (NS085097), and the Eli and Edythe Broad Center of Regenerative Medicine and Stem Cell Research at UCLA to S.J.B.

Received: August 2, 2017
Revised: December 14, 2017
Accepted: December 15, 2017
Published: January 11, 2018

REFERENCES

Andrews, M.G., Del Castillo, L.M., Ochoa-Bolton, E., Yamauchi, K., Smogorzewski, J., and Butler, S.J. (2017). BMPs direct sensory interneuron identity in the developing spinal cord using signal-specific not morphogenic activities. Elife *6*. https://doi.org/10.7554/eLife.30647.

Arber, S., Han, B., Mendelsohn, M., Smith, M., Jessell, T.M., and Sockanathan, S. (1999). Requirement for the homeobox gene Hb9 in the consolidation of motor neuron identity. Neuron *23*, 659–674.

Armour, B.S., Courtney-Long, E.A., Fox, M.H., Fredine, H., and Cahill, A. (2016). Prevalence and causes of paralysis - United States, 2013. Am. J. Public Health *106*, 1855–1857.

Bermingham, N.A., Hassan, B.A., Wang, V.Y., Fernandez, M., Banfi, S., Bellen, H.J., Fritzsch, B., and Zoghbi, H.Y. (2001). Proprioceptor pathway development is dependent on Math1. Neuron *30*, 411–422.

Bui, T.V., Akay, T., Loubani, O., Hnasko, T.S., Jessell, T.M., and Brownstone, R.M. (2013). Circuits for grasping: spinal dI3 interneurons mediate cutaneous control of motor behavior. Neuron *78*, 191–204.

Butler, S.J., and Bronner, M.E. (2015). From classical to current: analyzing peripheral nervous system and spinal cord lineage and fate. Dev. Biol. *398*, 135–146.

Bylund, M., Andersson, E., Novitch, B.G., and Muhr, J. (2003). Vertebrate neurogenesis is counteracted by Sox1-3 activity. Nat. Neurosci. *6*, 1162–1168.

Caspary, T., and Anderson, K.V. (2003). Patterning cell types in the dorsal spinal cord: what the mouse mutants say. Nat. Rev. Neurosci. *4*, 289–297.

Chizhikov, V.V., and Millen, K.J. (2004). Control of roof plate formation by Lmx1a in the developing spinal cord. Development *131*, 2693–2705.

Clark, A.T., Gkountela, S., Chen, D., Liu, W., Sosa, E., Sukhwani, M., Hennebold, J.D., and Orwig, K.E. (2017). Primate primordial germ cells acquire transplantation potential by Carnegie stage 23. Stem Cell Reports *9*, 329–341.

Diez del Corral, R., Olivera-Martinez, I., Goriely, A., Gale, E., Maden, M., and Storey, K. (2003). Opposing FGF and retinoid pathways control ventral neural pattern, neuronal differentiation, and segmentation during body axis extension. Neuron *40*, 65–79.

Dimos, J.T., Rodolfa, K.T., Niakan, K.K., Weisenthal, L.M., Mitsumoto, H., Chung, W., Croft, G.F., Saphier, G., Leibel, R., Goland, R., et al. (2008). Induced pluripotent stem cells generated from patients with ALS can be differentiated into motor neurons. Science *321*, 1218–1221.

Ebert, A.D., Yu, J., Rose, F.F., Jr., Mattis, V.B., Lorson, C.L., Thomson, J.A., and Svendsen, C.N. (2009). Induced pluripotent stem cells from a spinal muscular atrophy patient. Nature *457*, 277–280.

Ellis, P., Fagan, B.M., Magness, S.T., Hutton, S., Taranova, O., Hayashi, S., McMahon, A., Rao, M., and Pevny, L. (2004). SOX2, a persistent marker for multipotential neural stem cells derived from embryonic stem cells, the embryo or the adult. Dev. Neurosci. *26*, 148–165.

Engberg, N., Kahn, M., Petersen, D.R., Hansson, M., and Serup, P. (2010). Retinoic acid synthesis promotes development of neural progenitors from mouse embryonic stem cells by suppressing endogenous, Wnt-dependent nodal signaling. Stem Cells *28*, 1498–1509.

Forlani, S., Lawson, K.A., and Deschamps, J. (2003). Acquisition of Hox codes during gastrulation and axial elongation in the mouse embryo. Development *130*, 3807–3819.

Gerrard, L., Rodgers, L., and Cui, W. (2005). Differentiation of human embryonic stem cells to neural lineages in adherent culture by blocking bone morphogenetic protein signaling. Stem Cells *23*, 1234–1241.

Graham, V., Khudyakov, J., Ellis, P., and Pevny, L. (2003). SOX2 functions to maintain neural progenitor identity. Neuron *39*, 749–765.

Harper, J.M., Krishnan, C., Darman, J.S., Deshpande, D.M., Peck, S., Shats, I., Backovic, S., Rothstein, J.D., and Kerr, D.A. (2004). Axonal growth of embryonic stem cell-derived motoneurons in vitro and in motoneuron-injured adult rats. Proc. Natl. Acad. Sci. USA *101*, 7123–7128.

Hazen, V.M., Andrews, M.G., Umans, L., Crenshaw, E.B., 3rd, Zwijsen, A., and Butler, S.J. (2012). BMP receptor-activated Smads direct diverse functions during the development of the dorsal spinal cord. Dev. Biol. *367*, 216–227.

Helms, A.W., Battiste, J., Henke, R.M., Nakada, Y., Simplicio, N., Guillemot, F., and Johnson, J.E. (2005). Sequential roles for Mash1 and Ngn2 in the generation of dorsal spinal cord interneurons. Development *132*, 2709–2719.

Helms, A.W., and Johnson, J.E. (1998). Progenitors of dorsal commissural interneurons are defined by MATH1 expression. Development *125*, 919–928.

Hu, B.Y., Weick, J.P., Yu, J.Y., Ma, L.X., Zhang, X.Q., Thomson, J.A., and Zhang, S.C. (2010). Neural differentiation of human induced pluripotent stem cells follows developmental principles but with variable potency. Proc. Natl. Acad. Sci. USA *107*, 4335–4340.

Karumbayaram, S., Novitch, B.G., Patterson, M., Umbach, J.A., Richter, L., Lindgren, A., Conway, A.E., Clark, A.T., Goldman, S.A., Plath, K., et al. (2009). Directed differentiation of human-induced pluripotent stem cells generates active motor neurons. Stem Cells *27*, 806–811.

Keino-Masu, K., Masu, M., Hinck, L., Leonardo, E.D., Chan, S.S., Culotti, J.G., and Tessier-Lavigne, M. (1996). Deleted in Colorectal Cancer (DCC) encodes a netrin receptor. Cell *87*, 175–185.

Lai, H.C., Seal, R.P., and Johnson, J.E. (2016). Making sense out of spinal cord somatosensory development. Development *143*, 3434–3448.

Le Dreau, G., and Marti, E. (2012). Dorsal-ventral patterning of the neural tube: a tale of three signals. Dev. Neurobiol. *72*, 1471–1481.

Le Dreau, G., and Marti, E. (2013). The multiple activities of BMPs during spinal cord development. Cell. Mol. Life Sci. *70*, 4293–4305.

Lee, K.J., Dietrich, P., and Jessell, T.M. (2000). Genetic ablation reveals that the roof plate is essential for dorsal interneuron specification. Nature *403*, 734–740.

Li, X.J., Du, Z.W., Zarnowska, E.D., Pankratz, M., Hansen, L.O., Pearce, R.A., and Zhang, S.C. (2005). Specification of motoneurons from human embryonic stem cells. Nat. Biotechnol. *23*, 215–221.

Liem, K.F., Jr., Tremml, G., and Jessell, T.M. (1997). A role for the roof plate and its resident TGFbeta-related proteins in neuronal patterning in the dorsal spinal cord. Cell *91*, 127–138.

Mansouri, A., and Gruss, P. (1998). Pax3 and Pax7 are expressed in commissural neurons and restrict ventral neuronal identity in the spinal cord. Mech. Dev. *78*, 171–178.

Menezes, J.R.L., and Luskin, M.B. (1994). Expression of neuron-specific tubulin defines a novel population in the proliferative layers of the developing telencephalon. J. Neurosci. *14*, 5399–5416.

Miles, G.B., Yohn, D.C., Wichterle, H., Jessell, T.M., Rafuse, V.F., and Brownstone, R.M. (2004). Functional properties of motoneurons derived from mouse embryonic stem cells. J. Neurosci. *24*, 7848–7858.

Mitsui, K., Tokuzawa, Y., Itoh, H., Segawa, K., Murakami, M., Takahashi, K., Maruyama, M., Maeda, M., and Yamanaka, S. (2003). The homeoprotein Nanog is required for maintenance of pluripotency in mouse epiblast and ES cells. Cell *113*, 631–642.

Molotkova, N., Molotkov, A., Sirbu, I.O., and Duester, G. (2005). Requirement of mesodermal retinoic acid generated by Raldh2 for posterior neural transformation. Mech. Dev. *122*, 145–155.

Muller, T., Anlag, K., Wildner, H., Britsch, S., Treier, M., and Birchmeier, C. (2005). The bHLH factor Olig3 coordinates the specification of dorsal neurons in the spinal cord. Genes Dev. *19*, 733–743.

Nagasako, E.M., Oaklander, A.L., and Dworkin, R.H. (2003). Congenital insensitivity to pain: an update. Pain *101*, 213–219.

Novitch, B.G., Chen, A.I., and Jessell, T.M. (2001). Coordinate regulation of motor neuron subtype identity and pan-neuronal properties by the bHLH repressor Olig2. Neuron *31*, 773–789.

Pevny, L.H., Sockanathan, S., Placzek, M., and Lovell-Badge, R. (1998). A role for SOX1 in neural determination. Development *125*, 1967–1978.

Philippidou, P., and Dasen, J.S. (2013). Hox genes: choreographers in neural development, architects of circuit organization. Neuron *80*, 12–34.

Sabatier, C., Plump, A.S., Le, M., Brose, K., Tamada, A., Murakami, F., Lee, E.Y., and Tessier-Lavigne, M. (2004). The divergent Robo family protein rig-1/Robo3 is a negative regulator of slit responsiveness required for midline crossing by commissural axons. Cell *117*, 157–169.

Sances, S., Bruijn, L.I., Chandran, S., Eggan, K., Ho, R., Klim, J.R., Livesey, M.R., Lowry, E., Macklis, J.D., Rushton, D., et al. (2016). Modeling ALS with motor neurons derived from human induced pluripotent stem cells. Nat. Neurosci. *19*, 542–553.

Sareen, D., O'Rourke, J.G., Meera, P., Muhammad, A.K., Grant, S., Simpkinson, M., Bell, S., Carmona, S., Ornelas, L., Sahabian, A., et al. (2013). Targeting RNA foci in iPSC-derived motor neurons from ALS patients with a C9ORF72 repeat expansion. Sci. Transl. Med. *5*, 208ra149.

Spandidos, A., Wang, X., Wang, H., Dragnev, S., Thurber, T., and Seed, B. (2008). A comprehensive collection of experimentally

validated primers for polymerase chain reaction quantitation of murine transcript abundance. BMC Genomics *9*, 633.

Spandidos, A., Wang, X., Wang, H., and Seed, B. (2010). PrimerBank: a resource of human and mouse PCR primer pairs for gene expression detection and quantification. Nucleic Acids Res. *38*, D792–D799.

Suter, D.M., Tirefort, D., Julien, S., and Krause, K.H. (2009). A Sox1 to Pax6 switch drives neuroectoderm to radial glia progression during differentiation of mouse embryonic stem cells. Stem Cells *27*, 49–58.

Thomsen, G.M., Gowing, G., Svendsen, S., and Svendsen, C.N. (2014). The past, present and future of stem cell clinical trials for ALS. Exp. Neurol. *262* (Pt B), 127–137.

Tonge, P.D., and Andrews, P.W. (2010). Retinoic acid directs neuronal differentiation of human pluripotent stem cell lines in a non-cell-autonomous manner. Differentiation *80*, 20–30.

Tsuchida, T., Ensini, M., Morton, S.B., Baldassare, M., Edlund, T., Jessell, T.M., and Pfaff, S.L. (1994). Topographic organization of embryonic motor neurons defined by expression of LIM homeobox genes. Cell *79*, 957–970.

Varadarajan, S.G., and Butler, S.J. (2017). Netrin1 establishes multiple boundaries for axon growth in the developing spinal cord. Dev. Biol. *430*, 177–187.

Varadarajan, S.G., Kong, J.H., Phan, K.D., Kao, T.J., Panaitof, S.C., Cardin, J., Eltzschig, H., Kania, A., Novitch, B.G., and Butler, S.J. (2017). Netrin1 produced by neural progenitors, not floor plate cells, is required for axon guidance in the spinal cord. Neuron *94*, 790–799.e3.

Walther, C., and Gruss, P. (1991). Pax-6, a murine paired box gene, is expressed in the developing CNS. Development *113*, 1435–1449.

Wang, X., and Seed, B. (2003). A PCR primer bank for quantitative gene expression analysis. Nucleic Acids Res. *31*, e154.

Wichterle, H., Lieberam, I., Porter, J.A., and Jessell, T.M. (2002). Directed differentiation of embryonic stem cells into motor neurons. Cell *110*, 385–397.

Wichterle, H., and Peljto, M. (2008). Differentiation of mouse embryonic stem cells to spinal motor neurons. Curr. Protoc. Stem Cell Biol. *Chapter 1*, Unit 1H.1.1–1H.1.9.

Wine-Lee, L., Ahn, K.J., Richardson, R.D., Mishina, Y., Lyons, K.M., and Crenshaw, E.B., 3rd. (2004). Signaling through BMP type 1 receptors is required for development of interneuron cell types in the dorsal spinal cord. Development *131*, 5393–5403.

Wu, J.Q., Habegger, L., Noisa, P., Szekely, A., Qiu, C.H., Hutchison, S., Raha, D., Egholm, M., Lin, H.F., Weissman, S., et al. (2010). Dynamic transcriptomes during neural differentiation of human embryonic stem cells revealed by short, long, and paired-end sequencing. Proc. Natl. Acad. Sci. USA *107*, 5254–5259.

Yamauchi, K., Phan, K.D., and Butler, S.J. (2008). BMP type I receptor complexes have distinct activities mediating cell fate and axon guidance decisions. Development *135*, 1119–1128.

Yuengert, R., Hori, K., Kibodeaux, E.E., McClellan, J.X., Morales, J.E., Huang, T.W., Neul, J.L., and Lai, H.C. (2015). Origin of a Non-Clarke's column division of the dorsal spinocerebellar tract and the role of caudal proprioceptive neurons in motor function. Cell Rep. *13*, 1258–1271.

Stem Cell Reports, Volume *10*

Supplemental Information

Deriving Dorsal Spinal Sensory Interneurons from Human Pluripotent Stem Cells

Sandeep Gupta, Daniel Sivalingam, Samantha Hain, Christian Makkar, Enrique Sosa, Amander Clark, and Samantha J. Butler

Supplementary information

Supplementary Figure 1: Retinoic acid induces a cervical HOX profile in hEBs

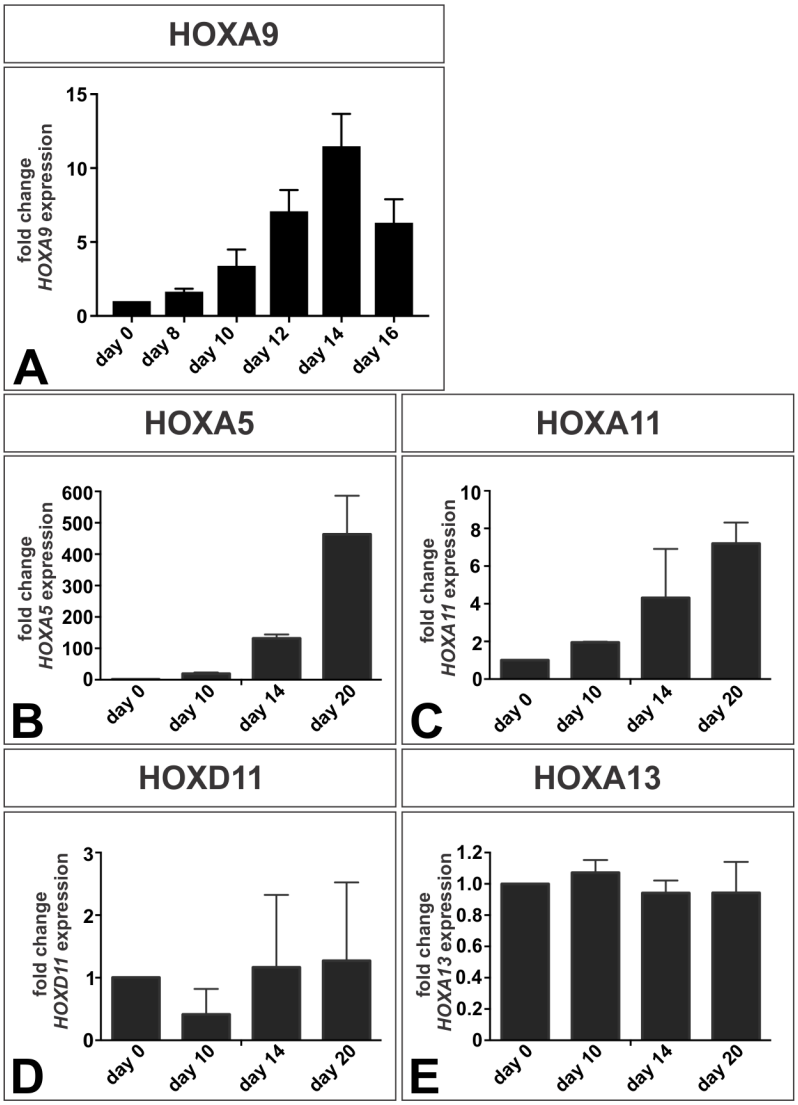

(A-E) RA-treated hEBs were assessed for the levels of *HOX* gene expression by RT-qPCR, which was normalized to day 0. By day 14-20 in the hESC differentiation protocol, there was significant increase in *HOXA9* (lower thoracic identity A, $p<0.04$, day 0 is similar to day 14), *HOXA5* (cervical level, B, $p<0.030$, day 0 versus day 20), and *HOXA11* (mid-lumbar level, C, $p<0.03$, day 0 versus day 20) expression in the hESC-derived EBs. There were no significant

changes in *HOXD11* (lower lumbar level, D, $p>0.84$, day 0 versus day 20) and HOXA13 (sacral level, E, $p>0.24$ for day 0 versus day 20).

Data are represented as mean±SEM. Two biological replicates were performed; the qRT-PCR conditions were run in triplicate.

Supplementary Figure 2: BMP4 suppresses the dI2 fate in hEBs.

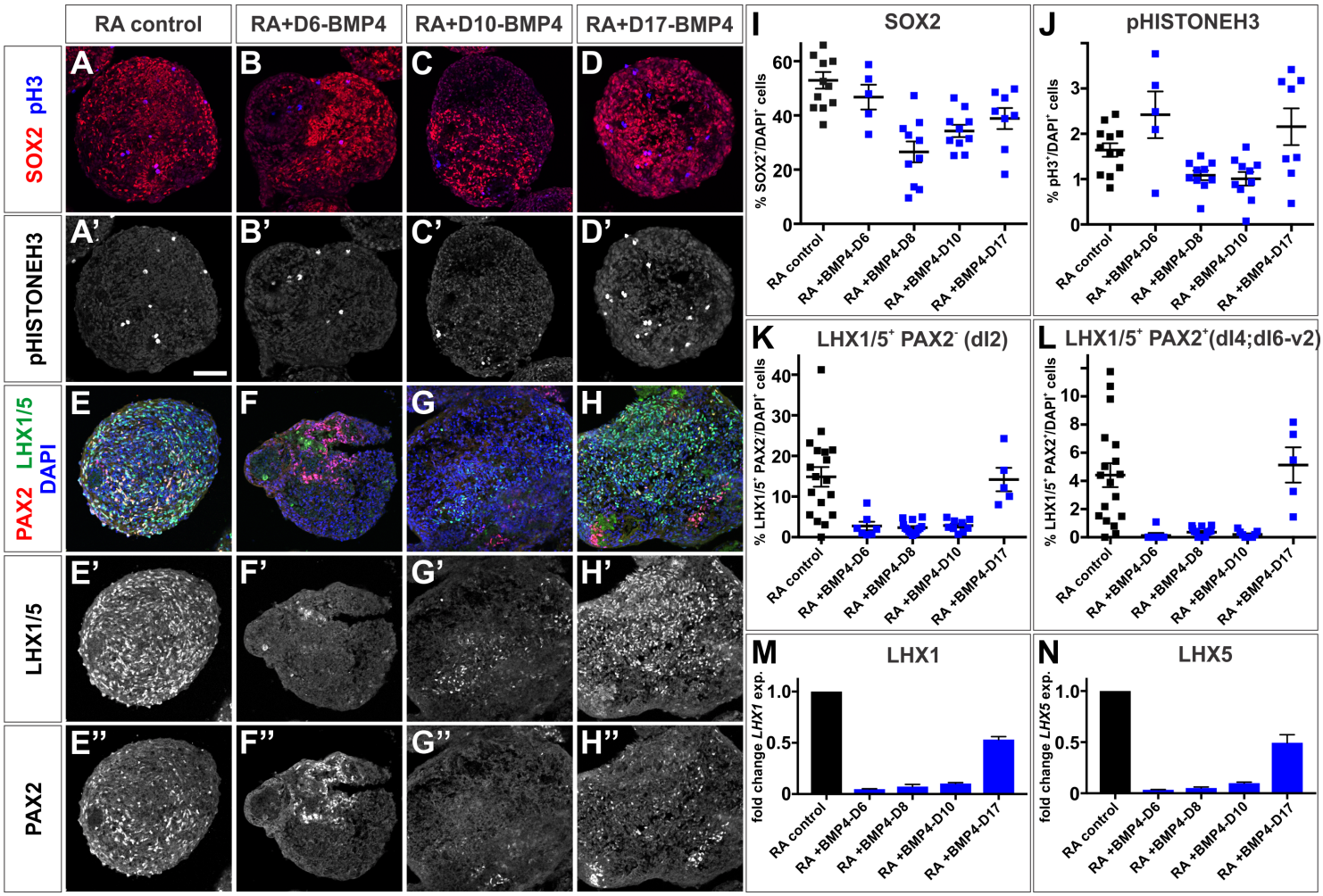

(A-D, I, J) By day 36 of the protocol, RA-treated hEBs still contain significant numbers of SOX2^{+} progenitors and phospho-HISTONEH3^{+} mitotic cells. The addition of BMP4, from day 8 on, significantly decreases the number of progenitors and dividing cells in hEBs (I, J; probability similar to RA control: $p<0.0001$, BMP4-D8; $p<0.0003$, BMP4-D10; $p<0.016$, BMP4-D17).

(E-H, K-N) RA treatment results in the generation of numerous LHX1/5^{+} PAX2^{-} cells (dI2) (E, E', K) and a few LHX1/5^{+} PAX2^{+} cells (dI4; dI6-v2) (E, E'', L). However, the specification of these cell types is suppressed by addition of BMP4 between day 6 and day 10 (dI2: F-G', K, $p<0.0015$, BMP4-D6; $p<0.0001$, BMP4-D8; $p<0.0005$, BMP4-D10; dI4, dI6-v2: $p<0.0001$ for all conditions) in hESCs derived EBs. By day 17, the addition of BMP4 no longer suppresses

dI2 identity (H-H", K; $p>0.9$, L; $p>0.48$). The effect of BMP4 on dI2 fates was also observed in an RT-qPCR analysis of *LHX1* and *LHX5* expression (M, N).

Data are represented as mean ± SEM. Two biological replicates were performed; the qRT-PCR conditions were run in triplicate and between 9-18 EBs were quantified for each condition, normalized to the total number of $DAPI^+$ cells and represented as the percent cell numbers. Scale bar=100 μm.

Supplementary Figure 3: Biological replicates for upregulation of LHX2 and ISL1 mRNA in the directed differentiation protocol

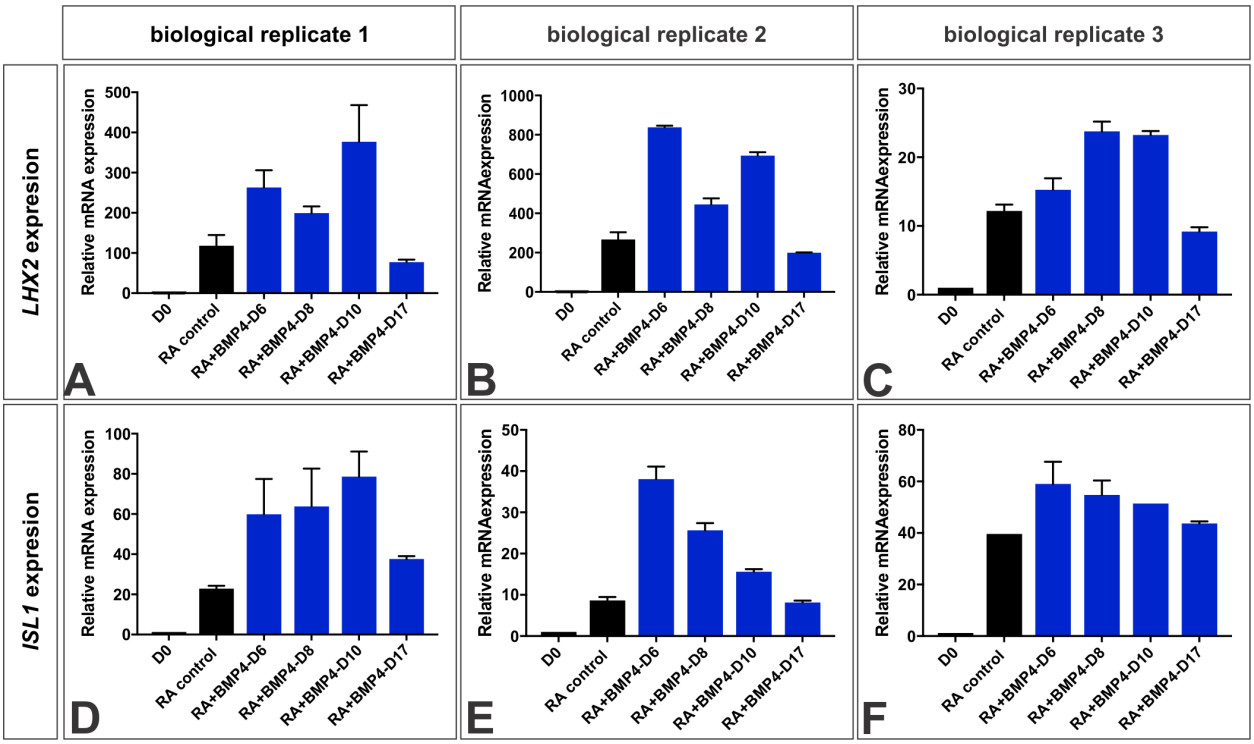

(A-F) RT-qPCR analysis of *LHX2* (A-C) and *ISL1* (D-F) expression in three biological replicates of the directed differention protocol. EBs were treated with RA, with BMP4 added at day 6, 8, 10 and 17. In each biological replicate *LHX2* and *ISL1* expression is upregulated after addition of BMP4, however there are marked differences in the magnitude of relative fold change. Three technical replicates were performed. Values are represented as mean±SEM.

Supplementary Figure 4: Characterization of hESC-derived mechanosensory dI3 cells

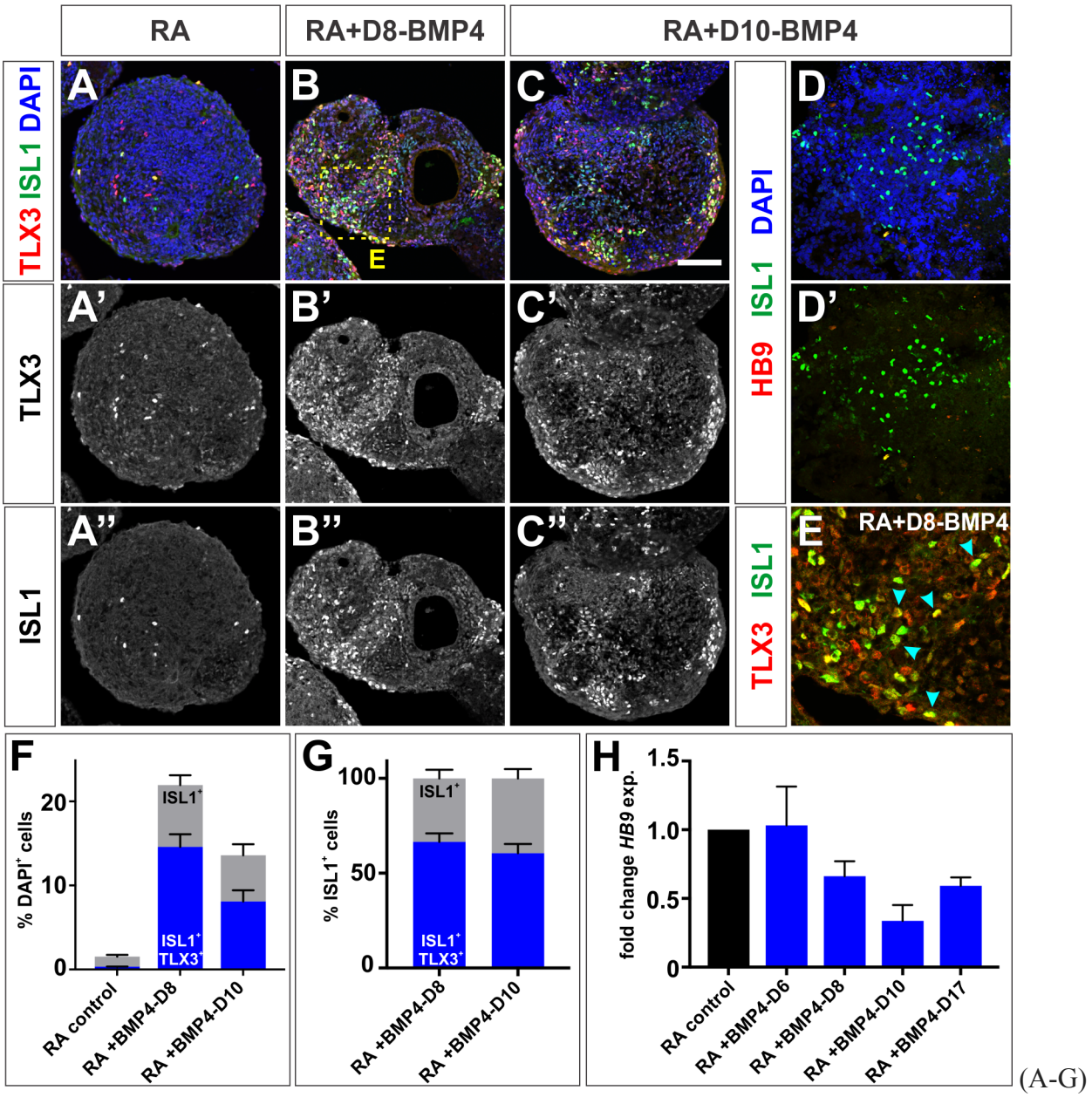

(A-G)

By day 36, BMP4 addition significantly increases the number of ISL1$^+$ TLX3$^+$ dI3 INs in the BMP4-D8 (B, E, $p<0.0001$ similar to RA control) and BMP4-D10 (C, $p<0.0001$) conditions compared to RA controls (A, F,). ~60% of dI3s are double positive for ISL1 and TLX3 (G). In contrast, the ISL1$^+$ cells are not co-labeled by the spinal motor neuron marker HB9 (D) and a RT-qPCR analysis showed that there was no *HB9* mRNA enrichment in any of the BMP4 conditions (H). Thus, the hESC-derived ISL1$^+$ cells no not have a motor neuron identity.

Data are represented as mean ± SEM. Two biological replicates were performed; the qRT-PCR conditions were run in triplicate and between 7-10 EBs were quantified for each condition. The number of $ISL1^+$ cells and $ISL1^+$ $TLX3^+$ cells were normalized to the number of $DAPI^+$ cells in D and to the total $ISL1^+$ cells in E.

Scale bar=100μm.

Table 1: Primary Antibodies

Antigen	Species	Dilution	Source
Sox2	Goat	1:1000	Santa Cruz Biotechnology (sc-17320)
Pax3	Goat	1:500	R&D Systems (AF2457)
Lhx2	Goat	1:250	Santa Cruz Biotechnology (sc-19344)
Isl1	Goat	1:500	R&D Systems (AF1837)
Sox1	Goat	1:500	Santa Cruz Biotechnology (sc-17318)
Pax6	Mouse	1:100	Developmental studies Hybridoma Bank (AB528427)
Nanog	Rabbit	1:200	Cell Signaling Technology (D73G4)
HoxA5	Goat	1:1000	Santa Cruz Biotechnology (sc-13199)
Olig2	Rabbit	1:300	Milipore (AB9610)
Tuj1	Mouse	1:1000	BioLegend (801202)
Dcc	Goat	1:200	R&D System (AF844)
Robo3	Goat	1:200	R&D System (AF3076)
Tlx3	Guinea pig	1:200	gift from Thomas Müller (Muller et al., 2005)
Lhx1/5	Mouse	1:20	Developmental Studies Hybridoma Bank
Pax2	Rabbit	1:500	Invitrogen

Table 2: RT-qPCR primer sequences

Gene name	Primer sequence
Nanog	For: CCCCAGCCTTTACTCTTCCTA Rev: CCAGGTTGAATTGTTCCAGGTC

Sox2	For: CAAAGAAAAACGAGGGAAATGGG Rev: TACCGGGTTTTCTCCATGCTG
Sox1	For: GCGGTAACAACTACAAAAAACTTGTAA Rev: GCGGAGCTCGTCGCATT
Pax6	For TTGAGCCATCACCAATCAGC Rev: TTTCTCCACGGATGTTGCTG
TUBB3 (β-III tubulin)	For: GGCCAAGGGTCACTACACG Rev: GCAGTCGCAGTTTTCACACTC
HoxA5	For: AAGTCATGACAACATAGGCGG Rev: TTCAATCCTCCTTCTGCGGG
Pax3	For: AGCACTGTACACCAAAGCAC Rev: AAAATCCATGCCTGGTGCTG
Olig2	For: CCCTAAAGGTGCGGATGCTT Rev: ACCCGAAAATCTGGATGCGA
Lhx2	For: TGGACCGAGGAACAACTTGG Rev: TCGCTCAGTCCACAAAACTG
Isl1	For: GATTTGGAATGGCATGCGGC Rev: GCGCATTTGATCCCGTACAA
Atoh1	For: ACCAGCTGCGCAATGTTATC Rev: TTTGTAGCAGCTCGGACAAG
Ascl1	For: AGCTTCTCGACTTCACCAACTG Rev: TGCTTCCAAAGTCCATTCGC
FoxD3	For: CGGCCTCGAGCAACAAATG Rev: AAATTGGGGAGAGGCAGAGTC
Lhx1	For: CAACATGCGCGTCATTCAGG Rev: ACTCGCTCTGGTAATCTCCG
Lhx5	For: GCGTCATCCAGGTGTGGTTT Rev: GGTGGACCCCAACATCTCAG

HoxA9	For: GTCCCACGCTTGACACTCA Rev: GCTGCTGGGTTATTGGGATCG
HoxD11	For: CAGCAGCGCAGTTGCC Rev: CGGTCAGTGAGGTTGAGCAT
HoxA13	For: CTGCCCTATGGCTACTTCGG Rev: CCGGCGGTATCCATGTACT
HoxA11	For: CCCGCAGTCTCGTCCAATTT Rev: AGGCTGTCTCGAAAAACTGGT

Table 3. Summary of the differentiation efficiencies.

	SOX2 (progenitor)	LHX2 (dI1)	LHX1/5^{+} PAX2^{-} (dI2)	ISL1 (dI3)	LHX1/5^{+} PAX2^{+} (dI4; dI6-v2)
RA	53%	8.5%	15%	1.5%	4.5%
RA+BMP4-D6	47%	26%	3%	15%	<0.2%
RA+BMP4-D8	26.5%	20%	2%	14.5%	<0.5%
RA+BMP4-D10	34%	18.5%	3%	8%	<0.2%
RA+BMP4-D17	39%	8%	14%	2%	5%